Impact of metal on the DNA photocleavage activity and cytotoxicity of ferrocenyl terpyridine 3d metal complexes

Basudev Maity, Sudarshan Gadadhar, Tridib K. Goswami, Anjali A. Karande* and Akhil R. Chakravarty*

Electronic Supplementary Information (ESI)†

Table of Content

Experimental

DNA binding experiment

The interaction of the compounds with double stranded calf thymus DNA was studied using 5 mM Tris-HCl or phosphate buffer medium. The ratio of the absorbance value of the DNA at 260 nm and 280 nm was 1.7:1 indicating that there were no protein impurities in the DNA samples. The concentrations of the CT DNA samples were measured by taking the molar absorption coefficient value of 6600 M^{-1} cm^{-1}.[1]

The intrinsic equilibrium binding constant (K_b) and the MvH fitting parameter (*s*, b.p.) of the complexes to calf thymus DNA were obtained from the UV-visible absorption titration method using 5 mM Tris-HCl buffer with a fixed complex concentration (15 μM for **1**-**4** and 25 μM for **5**). During titration, an equal quantity of DNA was added into the reference as well as sample solution to minimize the absorbance of DNA. The molar absorption coefficients from the spectra were calculated using Lambert-Beer law and fitted to the equation of Bard and coworkers based on McGhee-von Hippel (MvH) method : $\Delta\varepsilon_{af}/\Delta\varepsilon_{bf} = (b - (b^2 - 2K_b^2C_t[DNA]/s)^{½})/2K_b$, where $b = 1 + K_bC_t + K_b[DNA]/2s$, where C_t is the total concentration of the metal complex, *s* is the fitting parameter, ε_f, ε_a and ε_b are respectively the molar extinction coefficient values of the free complex in solution, complex bound to DNA at a definite concentration and the complex in completely bound form with CT DNA.[2] The non linear fitting of the data gave the value of K_b and s.

DNA melting experiments were carried out in 5 mM phosphate buffer (pH 6.8) containing 5% DMF. The DNA absorption band at 260 nm was monitored and the temperatures were varied from 40 to 90 °C at a scan rate of 1°C min^{-1} both in the absence and presence of the complexes.[3] The complex to DNA ratio was kept constant at 1:10. The melting temperatures (T_m) were calculated from the derivative of the DNA melting plot. Ethidium bromide was used as a standard DNA intercalator.

DNA cleavage experiment:

For DNA cleavage experiments plasmid supercoiled pUC19 DNA (0.2 μg, 30 μM, 2686 base pairs) was used and the experiments were carried out in 50 mM Tris-HCl buffer medium.

The 20 μL volume of the sample solution used for DNA photocleavage experiment was prepared by taking 1 μL SC pUC19 DNA, 1 μL 50 mM NaCl, 2 μL of the complex stock solution in DMF and 16 μL 50 mM tris-HCl buffer. For chemical nuclease experiments, an additional 2 μL of hydrogen peroxide or glutathione from 2 mM and 10 mM stock solutions, respectively, was used. For mechanistic investigations for the DNA photocleavage reactions the samples were prepared in the presence of various external additives, viz. KI (50 mM), NaN_3 (50 mM), TEMP (50 mM), DMSO (8 μL), SOD (150 unit) and catalase (100 units). Distamycin (4 mM) as DNA minor groove binder was used to study the groove binding nature by the complexes. The light sources used for the DNA photocleavage reactions were an UV-A lamp for 365 nm (6 W, sample area of illumination = 45 mm^2) and a continuous wave (CW) Ar-Kr laser (100 mW, laser beam diameter = 1.8 mm, beam divergence = 0.7 mrad, Spectra Physics water-cooled mixed-gas ion laser Stabilite 2018-RM) for visible light. The power of the laser beam was measured using a Spectra Physics CW laser power meter (model 407A). The solution path length used for illumination in the glass vial was ~5 mm. Before photo-exposure the sample solutions were incubated at 37 °C for 1h. For chemical nuclease experiments the sample solutions were incubated for 2 h at 37 °C. After photoexposure, a 2 μL solution of the loading dye containing 30 mM EDTA, 0.05% bromophenol blue, 0.05% xylene cynol and 36% glycerol was added to quench the reaction. Agarose gel (1%, containing 1.0 μg ml^{-1} ethidium bromide) electrophoresis was carried out in a dark room for 2 h at 45 V in 1X TAE (Tris-acetate-EDTA) buffer. The conversion of supercoiled (SC) to nicked circular (NC) DNA was visualized by UV light and the intensities of each form were measured by using a UVITECH Gel Documentation System.[4] The observed error in measuring the band intensities was ~5-7%.

References

(1) M. E. Reichman, S. A. Rice, C. A. Thomas and P. Doty, *J. Am. Chem. Soc.*, 1954, **76**, 3047.

(2) J. D. McGhee and P. H. Von Hippel, *J. Mol. Biol.*, 1974, **86**, 469.

(3) M. T. Carter, M. Rodriguez and A. J. Bard, *J. Am. Chem. Soc.*, 1989, **111**, 8901.

(4) J. Bernadou, G. Pratviel, F. Bennis, M. Girardet and B. Meunier, *Biochemistry*, 1989, **28**, 7268.

Table S1. The ^{1}H-NMR chemical shift values for the complexes **1**, **4**-**6** in DMSO-d_6 solvent (s, singlet; d, doublet; t, triplet; pst, pseudotriplet; m, multiplet)

Complexes	δ in ppm
$[Fe(Fc\text{-}tpy)_2](ClO_4)_2$, **1**	9.32(s, 4H), 9.0(d, *J* = 8.0, 4H), 8.03(m, 4H), 7.23(d, *J* = 4.4 Hz, 8H), 5.66(pst, *J* = 1.6 Hz, 4H), 4.86(pst, *J* = 1.6 Hz, 4H), 4.41(s, 10H)
$[Zn(Fc\text{-}tpy)_2](ClO_4)_2$, **4**	9.07(d, *J* = 8.0 Hz, 4H), 8.99(s, 4H), 8.26(t, *J* = 4.4 Hz, 4H), 7.90(d, *J* = 4.8 Hz, 4H), 7.49(t, *J* = 7.2 Hz, 4H), 5.63(pst, *J* = 1.6 Hz, 4H), 4.82(pst, *J* = 1.8 Hz, 4H), 4.29(s, 10H)
$[Zn(Ph\text{-}tpy)_2](ClO_4)_2$, **5**	9.38(s, 4H) 9.14(d, *J* = 8.0, 4H), 8.41(d, *J* = 7.2 Hz, 4H), 8.26(t, *J* = 7.6 Hz, 4H), 7.94(d, *J* = 4.4 Hz, 4H), 7.76-7.70(m, 6H), 7.47(t, *J* = 6.2 Hz, 4H)
$[Zn(Fc\text{-}dpa)_2](ClO_4)_2$, **6**	8.60(d, *J* = 3.6 Hz, 2H), 8.46(d, *J* = 4.0, 2H), 8.06(t, *J* = 7.2 Hz, 2H), 7.75(t, *J* = 7.2 Hz, 2H), 7.62-7.50(m, 6H), 7.22(t, *J* = 6.4 Hz, 2H), 4.38(s, 2H), 4.30(s, 2H), 4.20(s, 2H), 4.9(s, 7H), 4.0(s, 5H), 3.61(s, 8H), 3.53(s, 2H), 3.46(s, 2H)

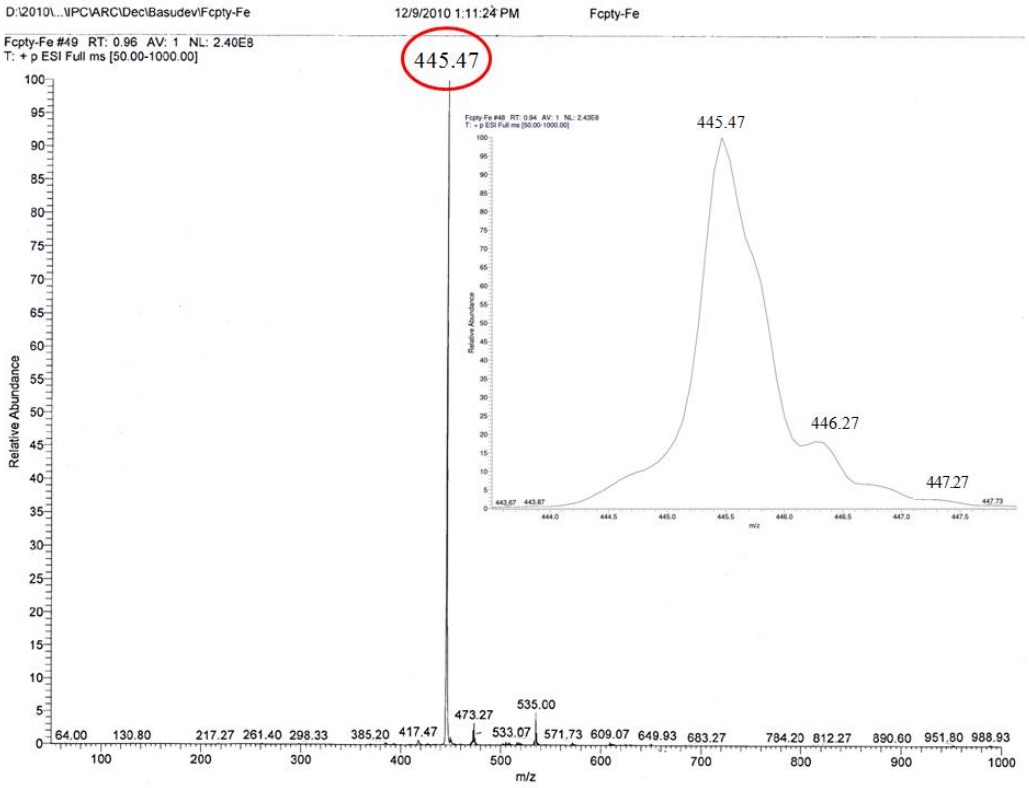

Figure S1: The ESI-MS spectrum of $[Fe(Fc\text{-}tpy)_2](ClO_4)_2$ (**1**) in MeCN showing essentially the parent ion peak (m/z) at 445.47 which corresponds to $[M\text{-}2(ClO_4)]^{2+}$.

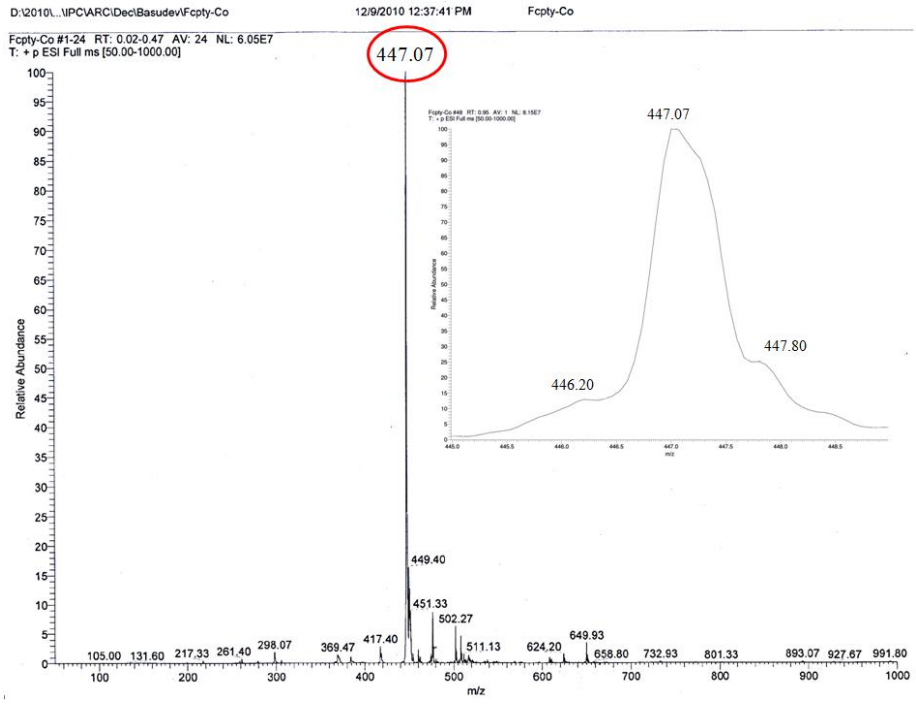

Figure S2: The ESI-MS spectrum of $[Co(Fc\text{-}tpy)_2](ClO_4)_2$ (**2**) in MeCN showing essentially the parent ion peak (m/z) at 447.07 which corresponds to $[M\text{-}2(ClO_4)]^{2+}$.

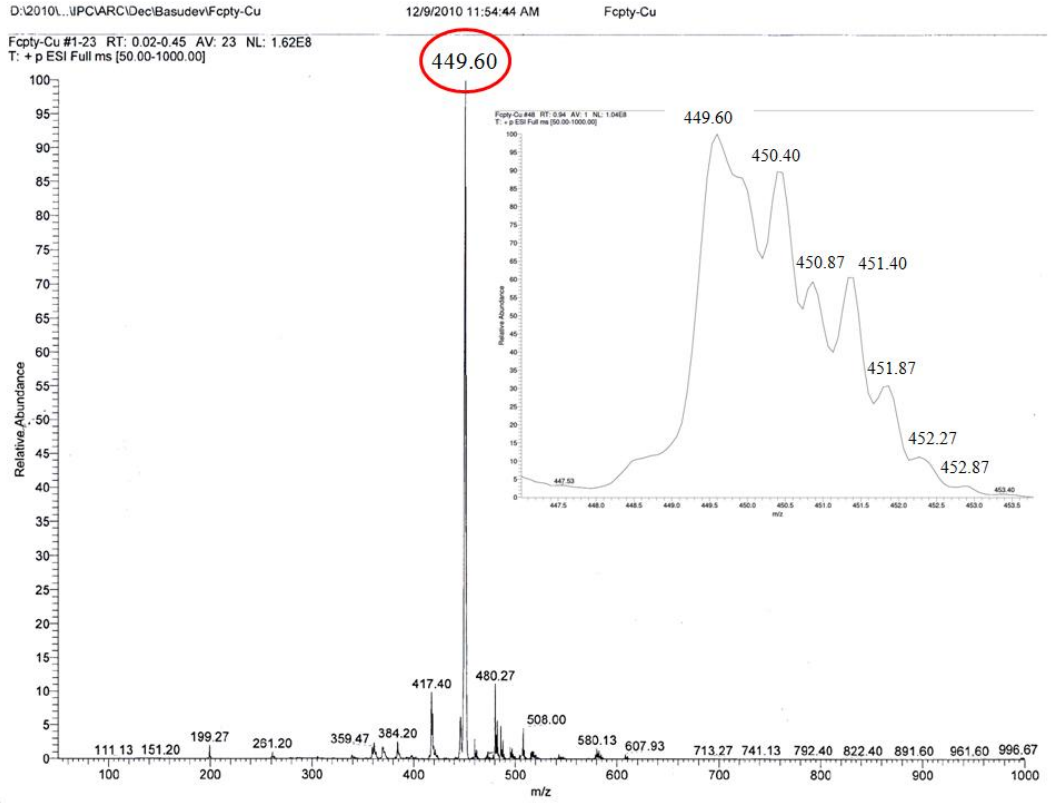

Figure S3: The ESI-MS spectrum of $[Cu(Fc\text{-}tpy)_2](ClO_4)_2$ (**3**) in MeCN showing prominent parent ion peak (m/z) at 449.60 which corresponds to $[M\text{-}2(ClO_4)]^{2+}$.

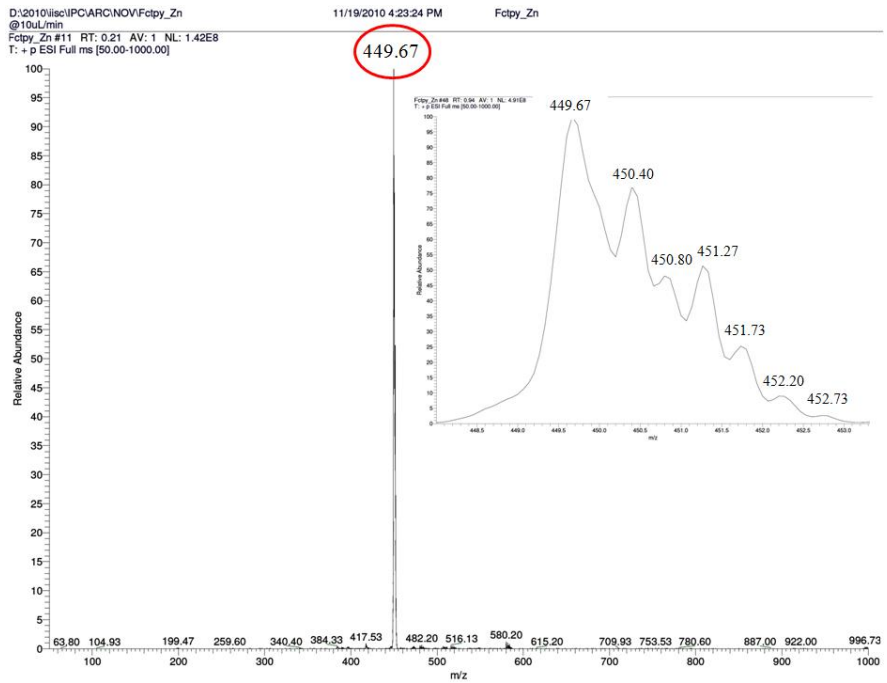

Figure S4: The ESI-MS spectrum of $[Zn(Fc\text{-}tpy)_2](ClO_4)_2$ (**4**) in MeCN showing prominent parent ion peak (m/z) at 449.67 which corresponds to $[M\text{-}2(ClO_4)]^{2+}$.

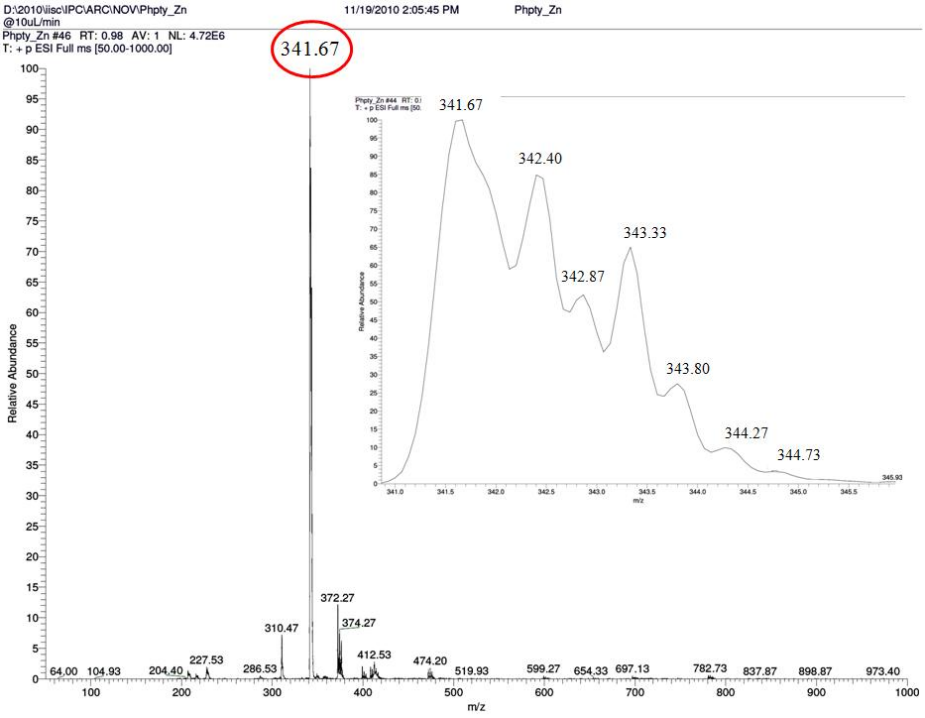

Figure S5: The ESI-MS spectrum of $[Zn(Ph\text{-}tpy)_2](ClO_4)_2$ (**5**) in MeCN showing prominent parent ion peak (m/z) at 341.67 which corresponds to $[M\text{-}2(ClO_4)]^{2+}$.

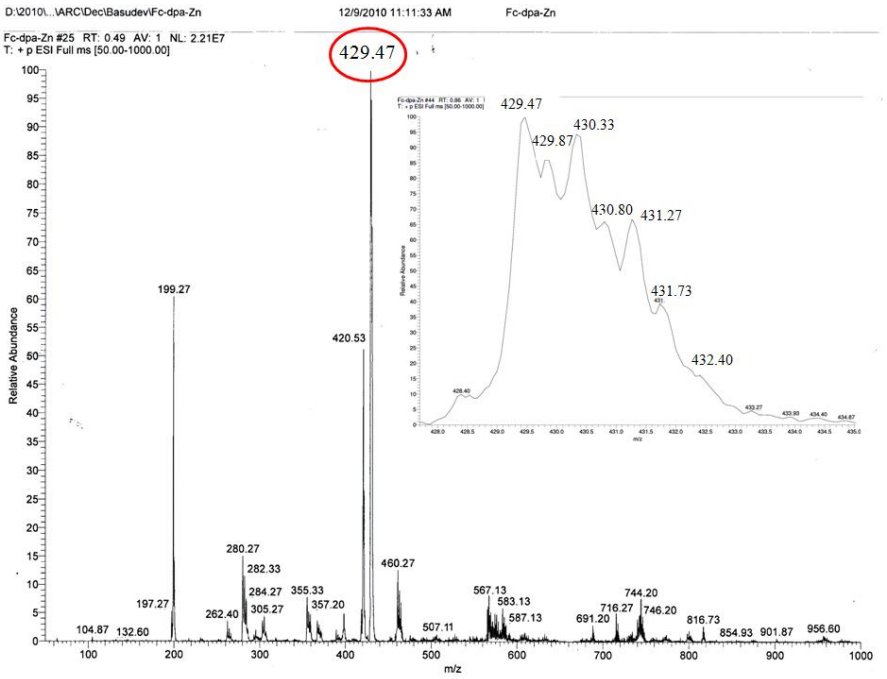

Figure S6: The ESI-MS spectrum of $[Zn(Fc\text{-}dpa)_2](ClO_4)_2$ (**6**) in MeCN showing the parent ion peak (m/z) at 429.47 which corresponds to $[M\text{-}2(ClO_4)]^{2+}$. Peaks at 199 and 420 correspond to $[FcCH_2]^+$ and $[Fc\text{-}dpa + Na]^+$, respectively.

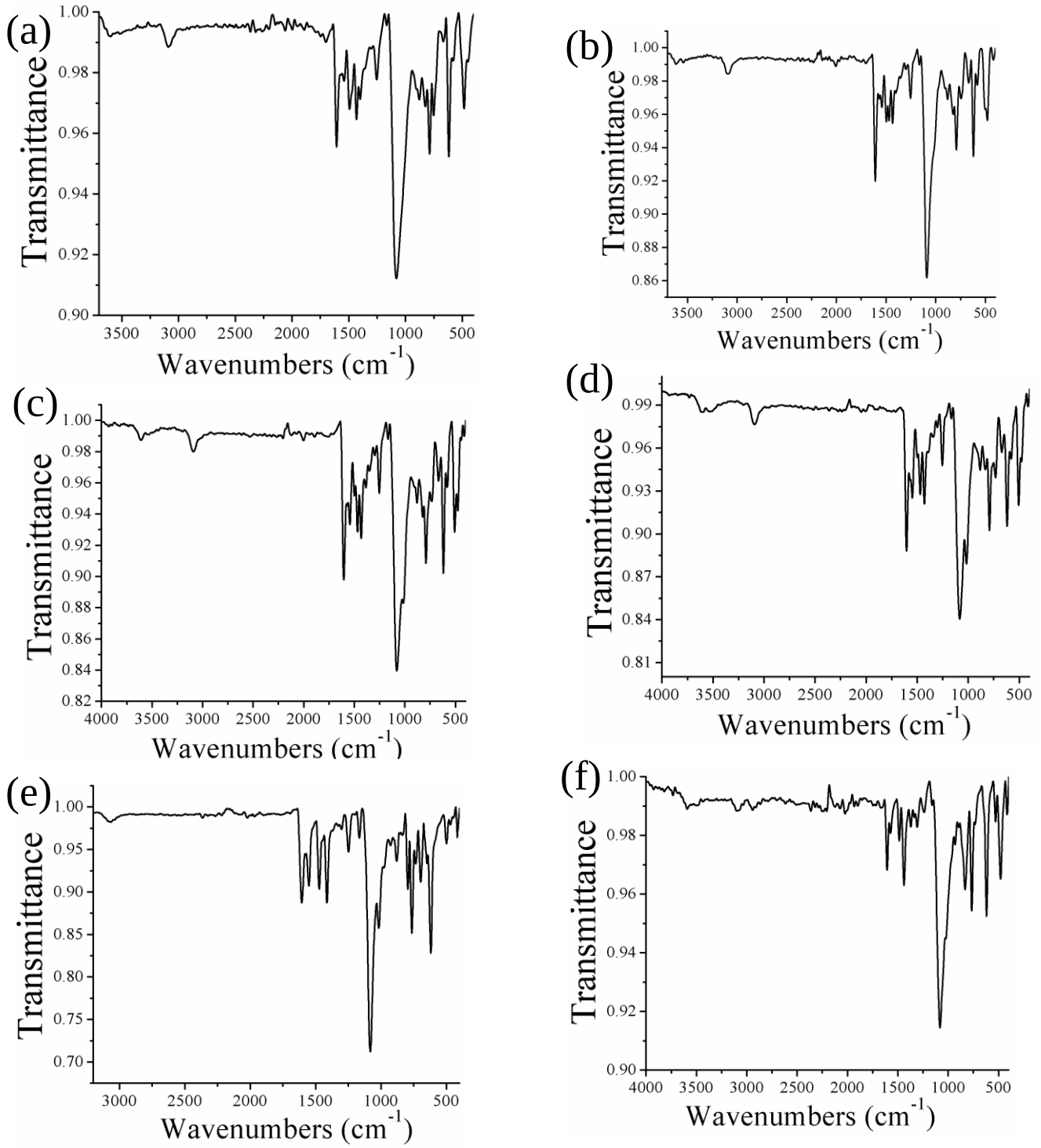

Figure S7: IR spectra of the complexes $[Fe(Fc\text{-}tpy)_2](ClO_4)_2$ (**1**) (a), $[Co(Fc\text{-}tpy)_2](ClO_4)_2$ (**2**) (b), $[Cu(Fc\text{-}tpy)_2](ClO_4)_2$ (**3**) (c), $[Zn(Fc\text{-}tpy)_2](ClO_4)_2$ (**4**) (d), $[Zn(Ph\text{-}tpy)_2](ClO_4)_2$ (**5**) (e), $[Zn(Fc\text{-}dpa)_2](ClO_4)_2$ (**6**) (f).

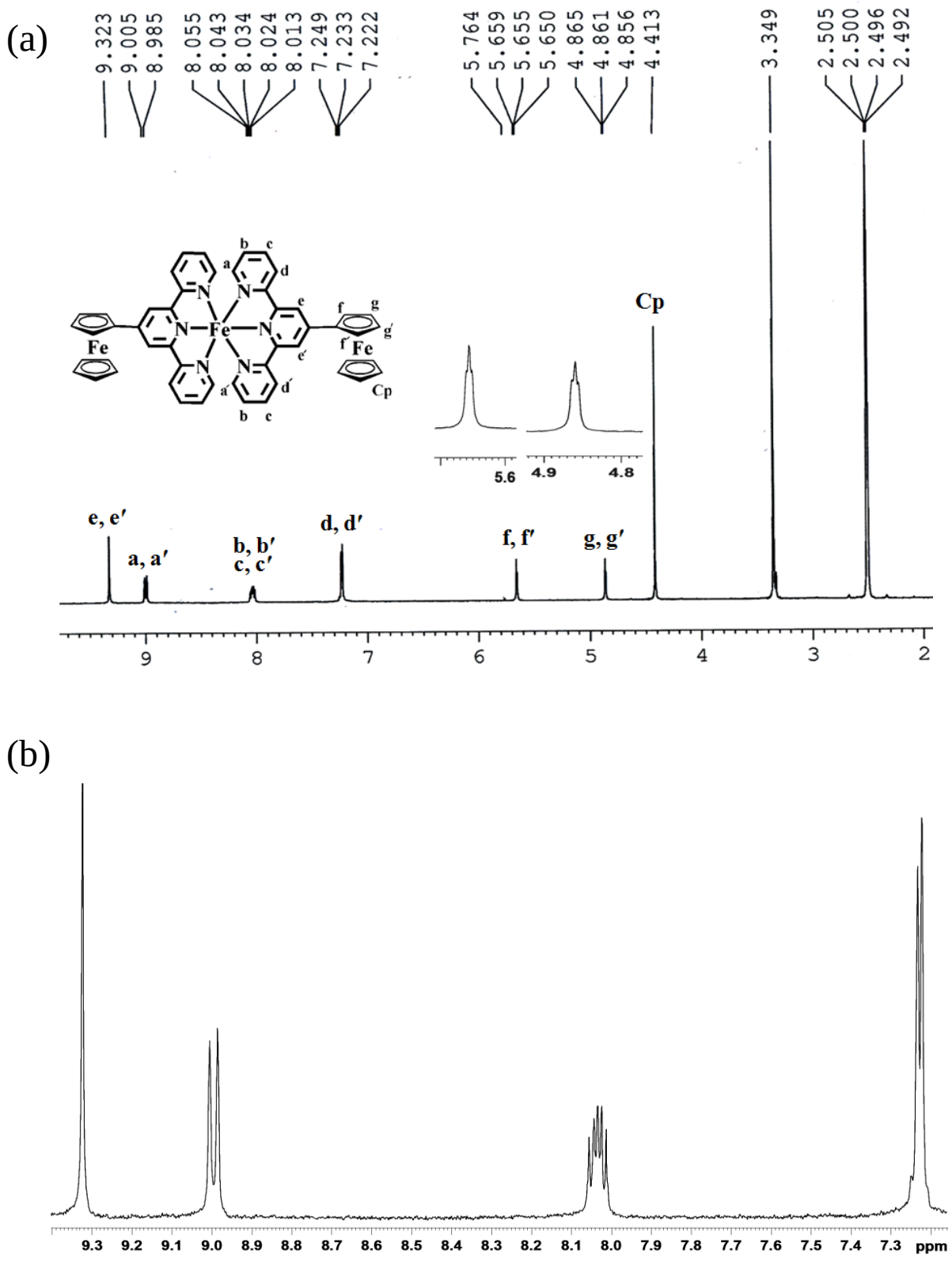

Figure S8. ^{1}H NMR spectrum (a) of **1** in DMSO – d_6 solvent (a) and the expansion of the aromatic region(b).

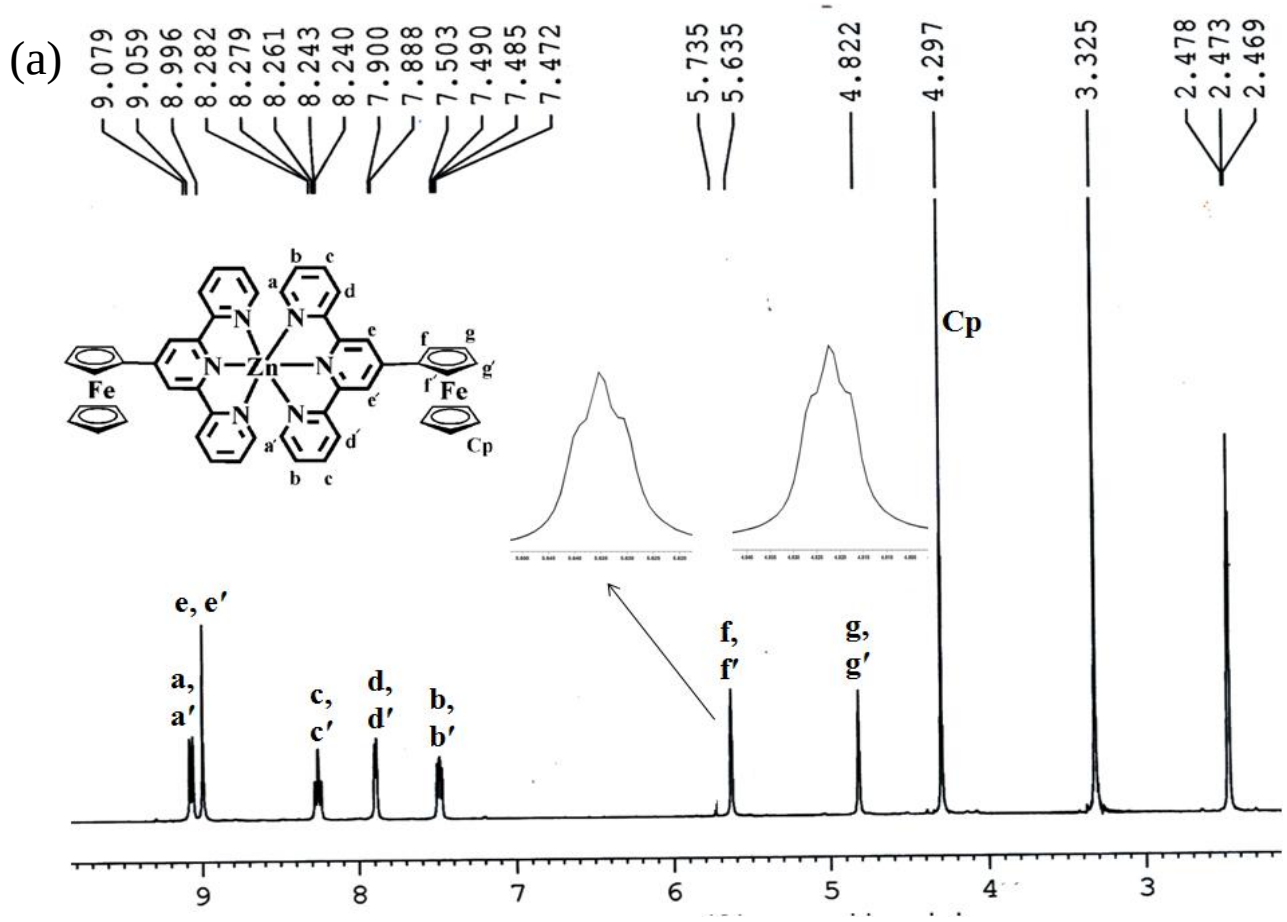

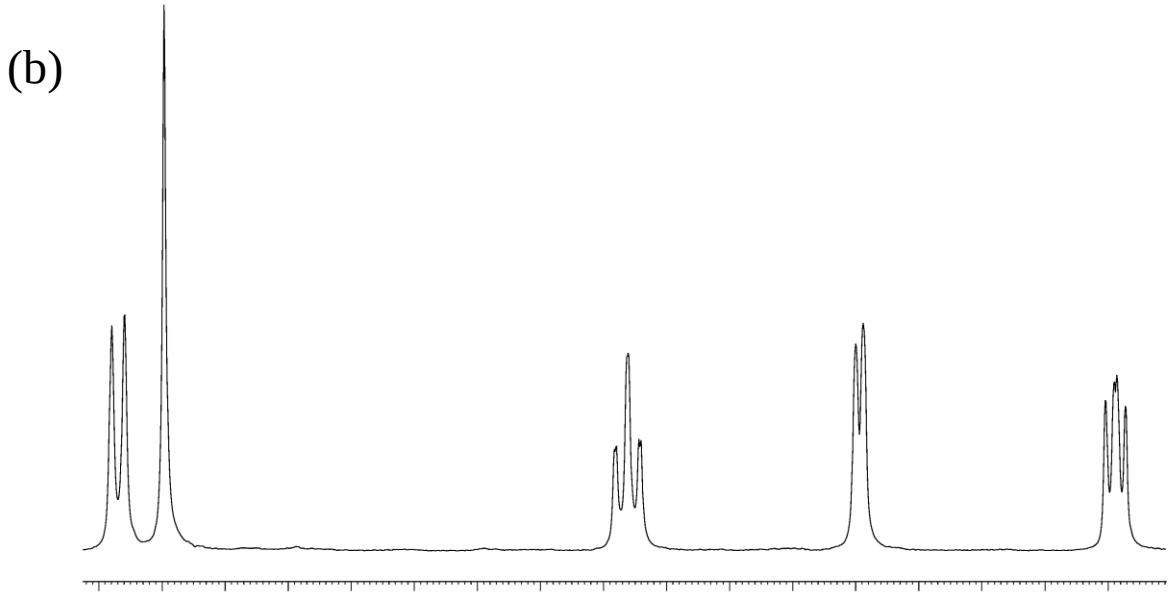

Figure S9. ^{1}H NMR spectrum (a) of **4** in DMSO – d_6 solvent (a) and the expansion of the aromatic region(b).

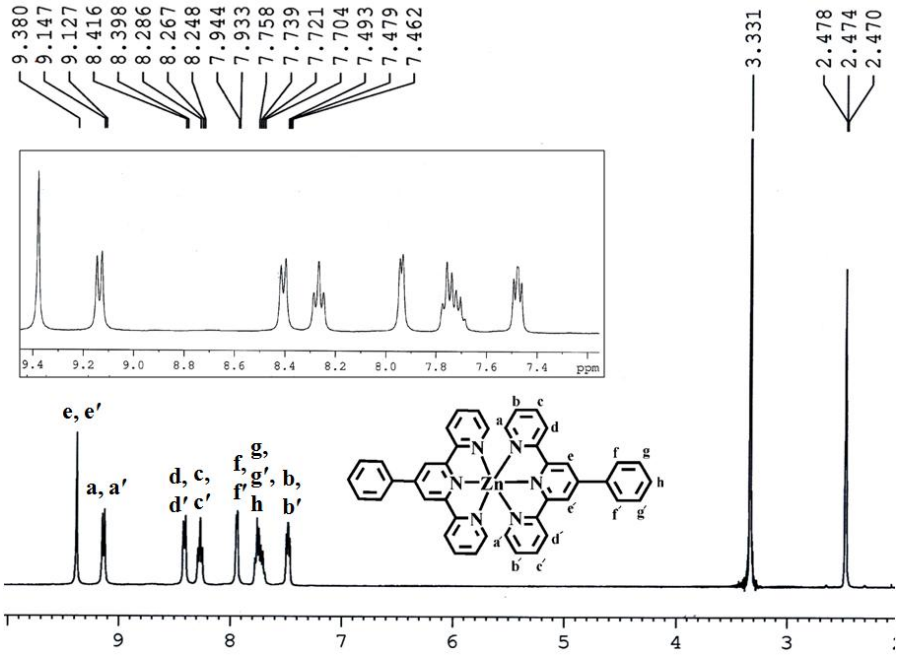

Figure S10. ^{1}H NMR spectrum of **5** in DMSO – d_6 solvent. The inset shows the expansion of the aromatic region.

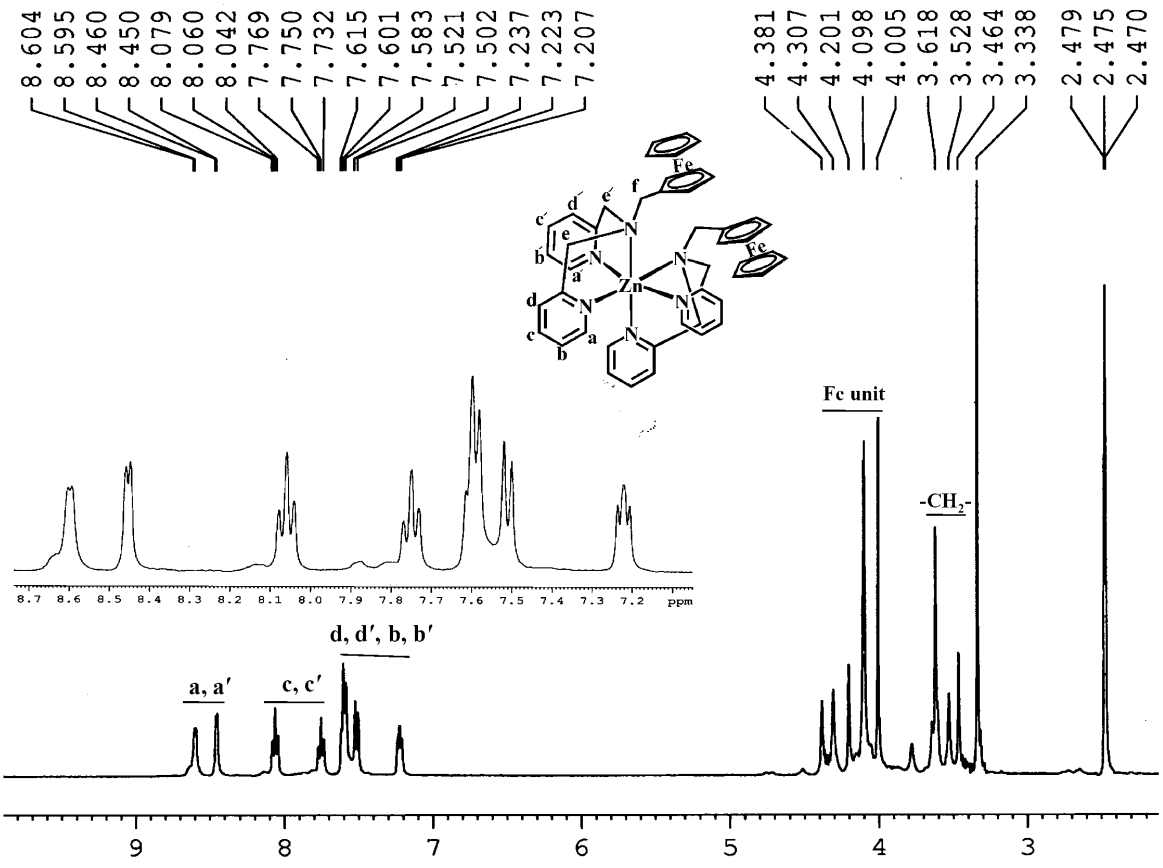

Figure S11. ^{1}H NMR spectrum of **6** in DMSO – d_6 solvent.

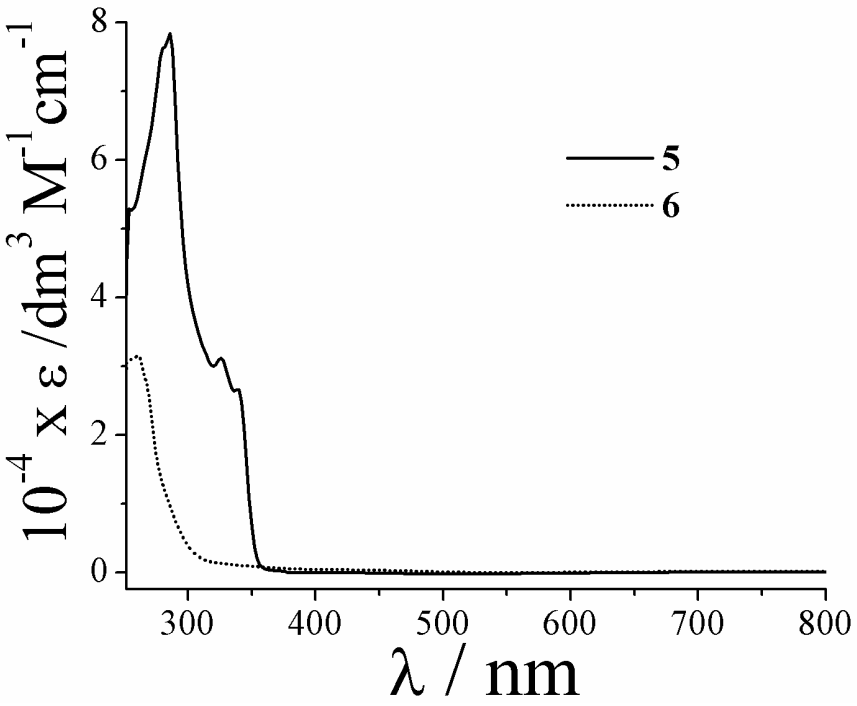

Figure S12: UV- visible absorption spectra for the complexes **5** and **6** in 50% aqueous DMF.

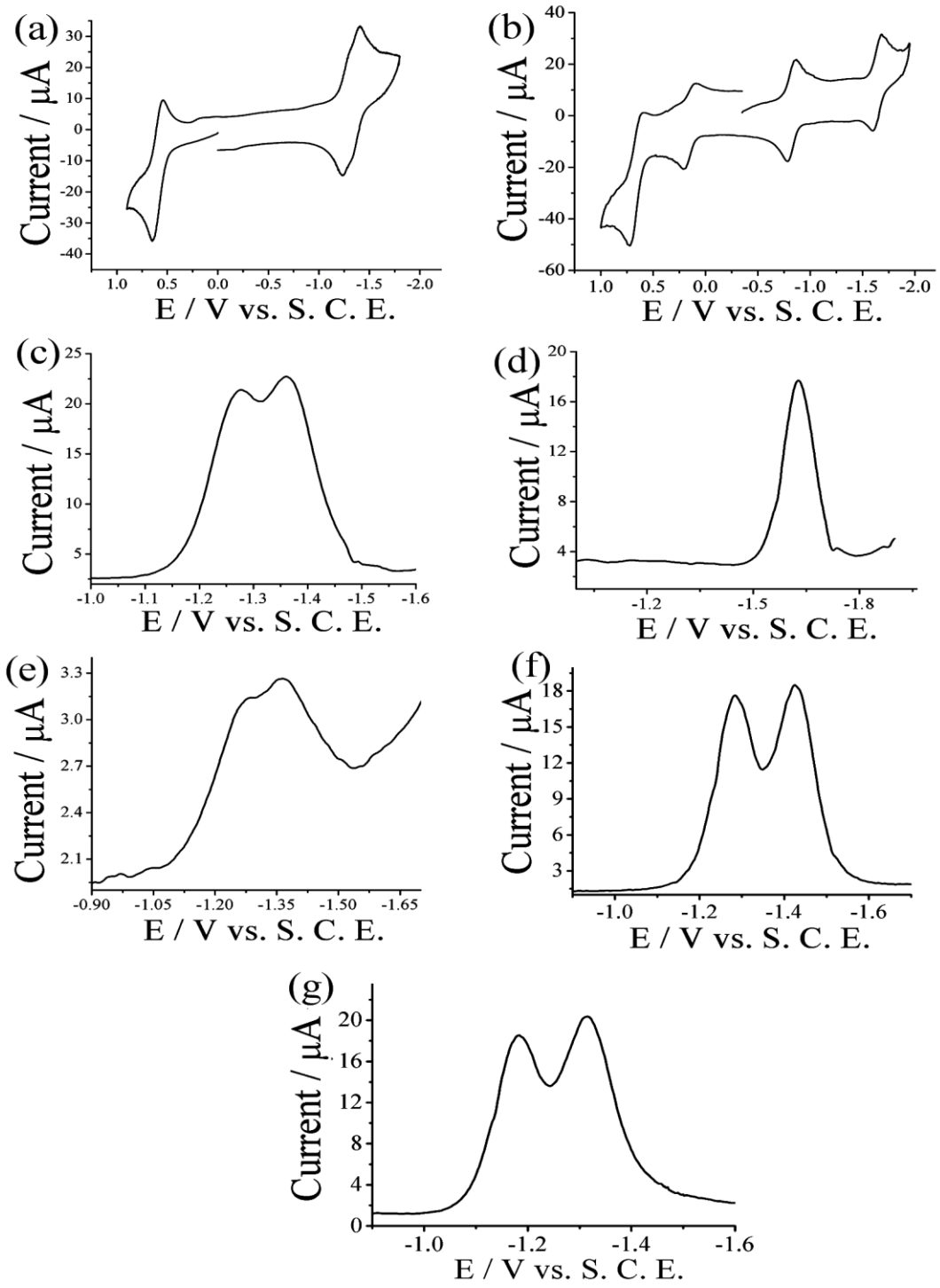

Figure S13: Cyclic voltammograms showing the Fc^{+}-Fc redox couple and ligand reduction of the complex **1** (a) and the Fc^{+}-Fc, Co(III)-Co(II) and Co(II)-Co(I) redox couples in **2** (b). The differential pulse voltammograms (DPV) for the ligand reductions in the complexes are shown for **1** (c), **2** (d), **3** (e), **4** (f) and **5** (g).

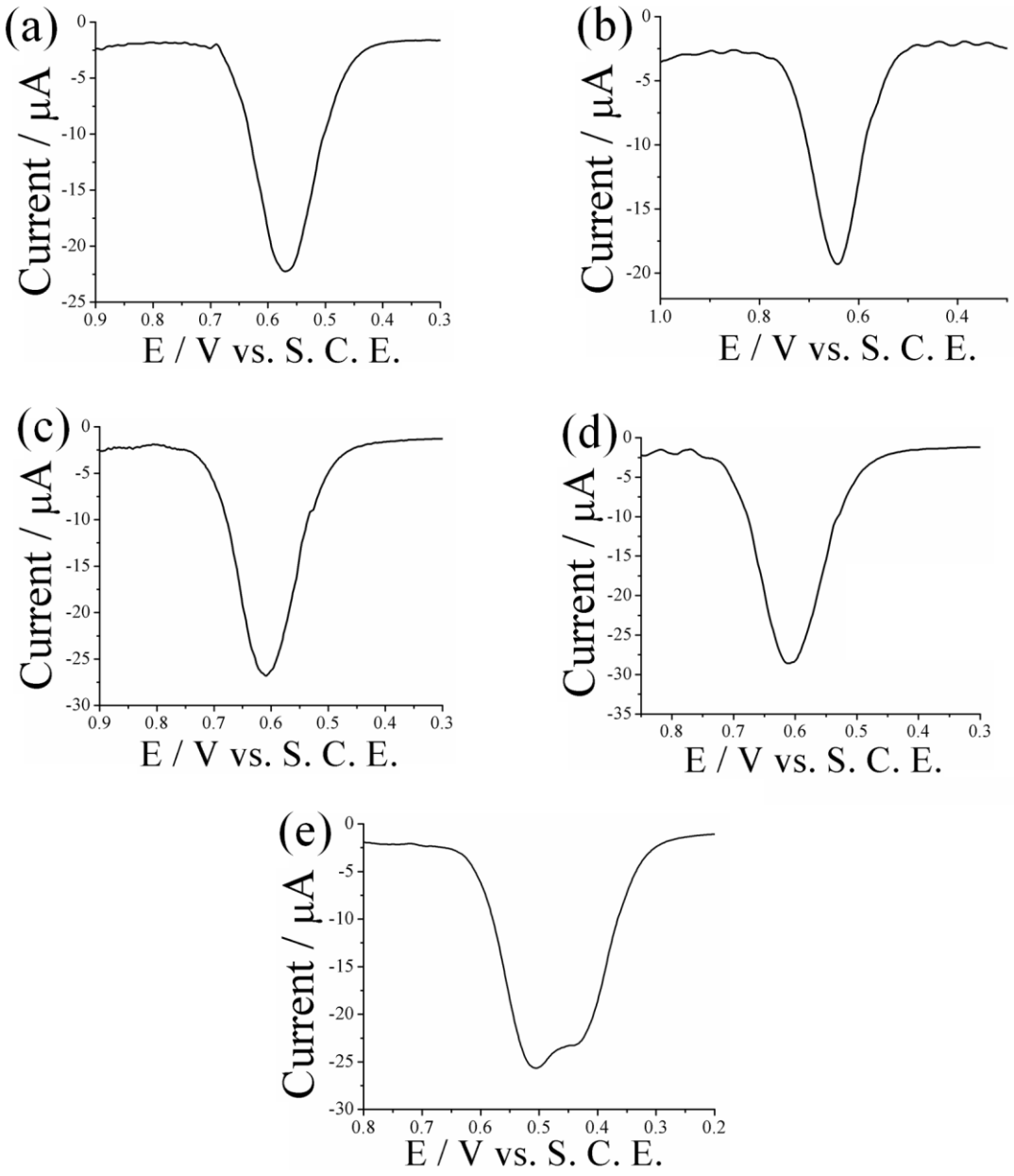

Figure S14: The differential pulse voltammograms (DPV) showing the ferrocenyl oxidation Fc → Fc^+ peak in **1** (a), **2** (b), **3** (c), **4** (d) and **6** (e).

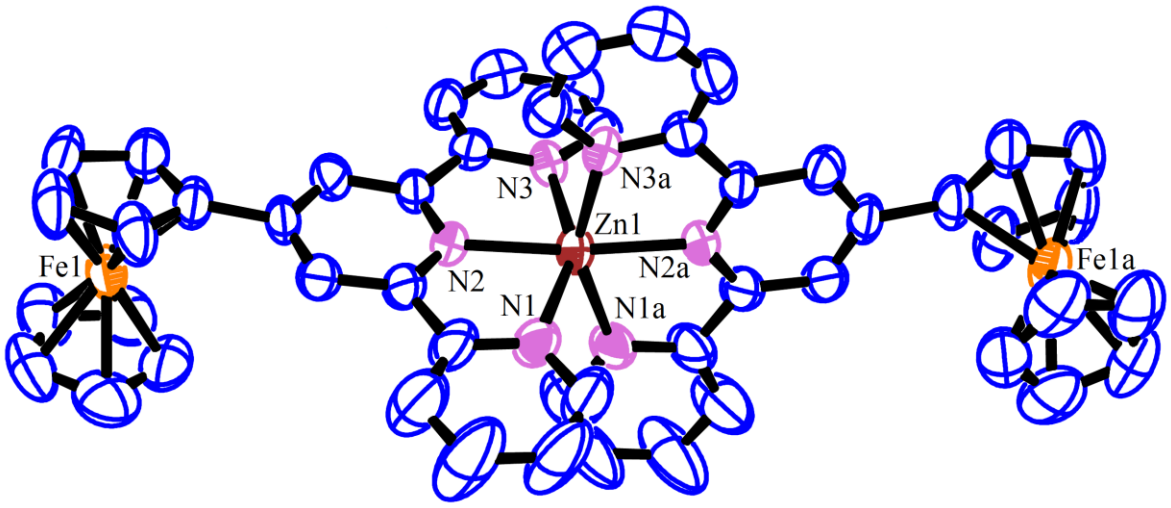

Figure 15. An ORTEP view of the cationic complex in **4** showing 50% probability thermal ellipsoids and the atom numbering scheme for the metal and hetero atoms. The hydrogen atoms are not shown for clarity.

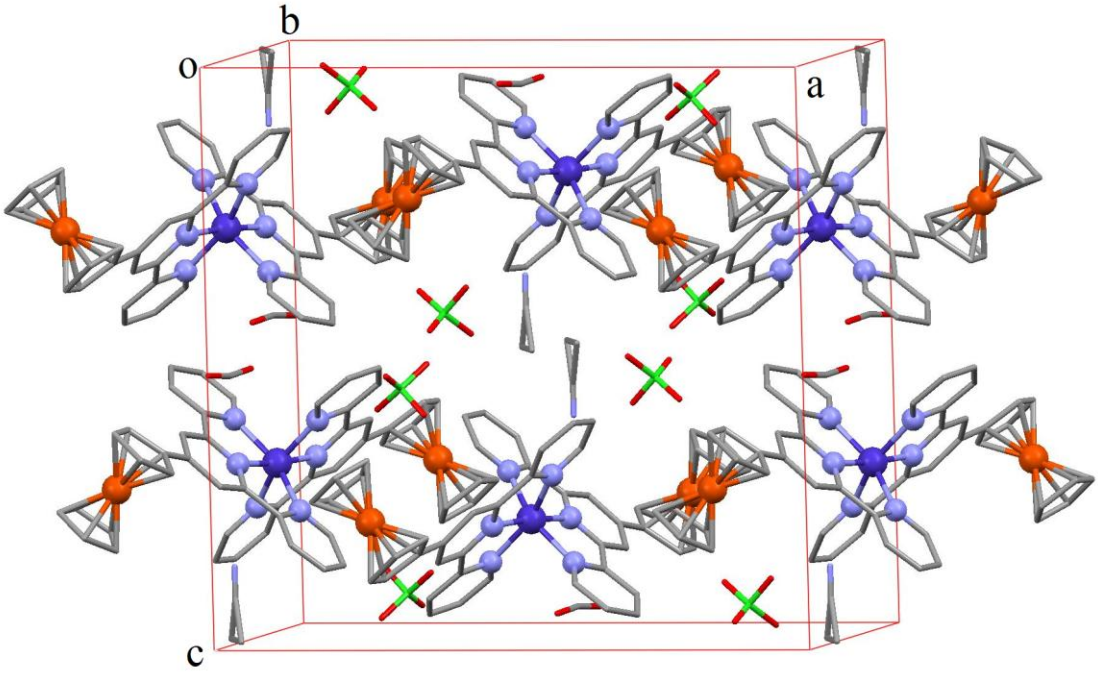

Figure S16: Unit cell packing diagram for the complex $[Co(Fc\text{-}tpy)_2](ClO_4)_2.MeOH.MeCN$. The complex crystallized in monoclinic *C*2/c space group with $Z = 4$. The hydrogen atoms are not shown for clarity.

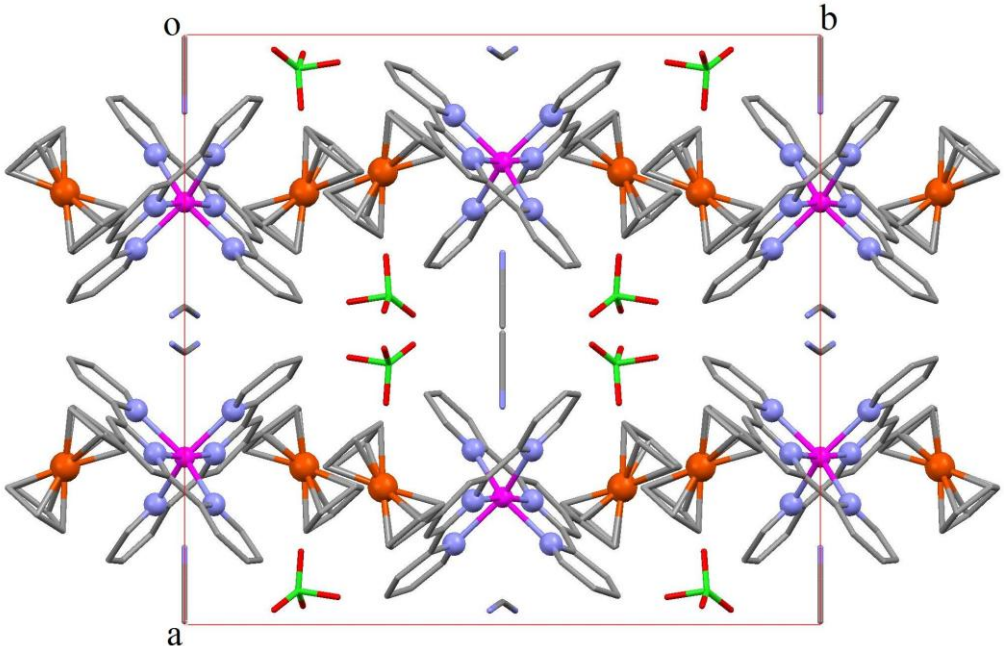

Figure S17: Unit cell packing diagram for the complex $[Zn(Fc\text{-}tpy)_2](ClO_4)_2.2MeCN$ along c axis. The complex crystallized in monoclinic *C*2/c space group with $Z = 4$. The hydrogen atoms are not shown for clarity.

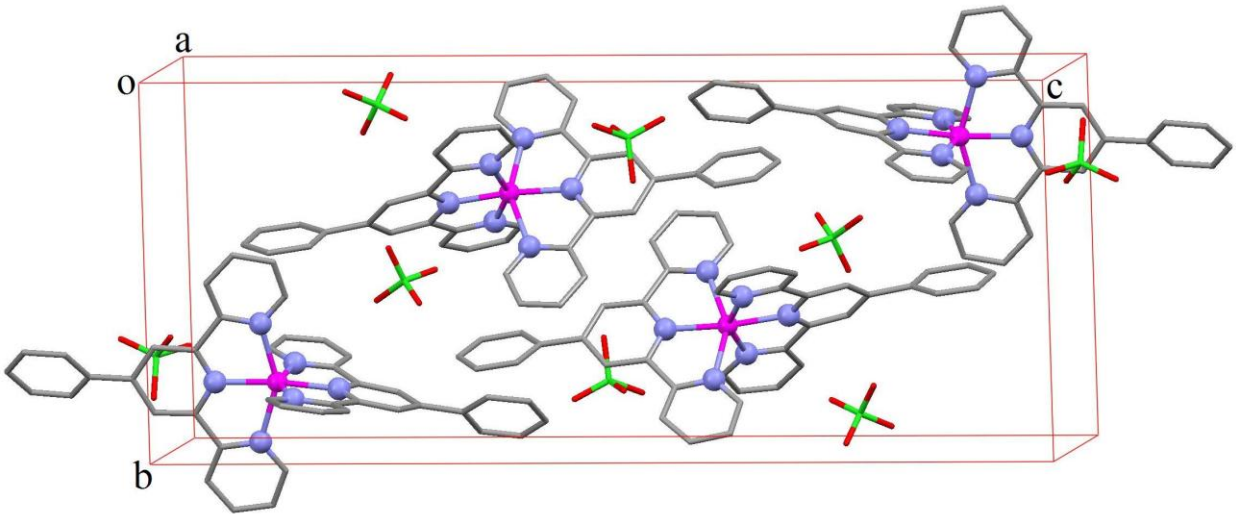

Figure S18: Unit cell packing diagram for the complex $[Co(Fc\text{-}tpy)_2](ClO_4)_2$. The complex crystallized in monoclinic $P2_1/c$ space group with $Z = 4$. The hydrogen atoms are not shown for clarity.

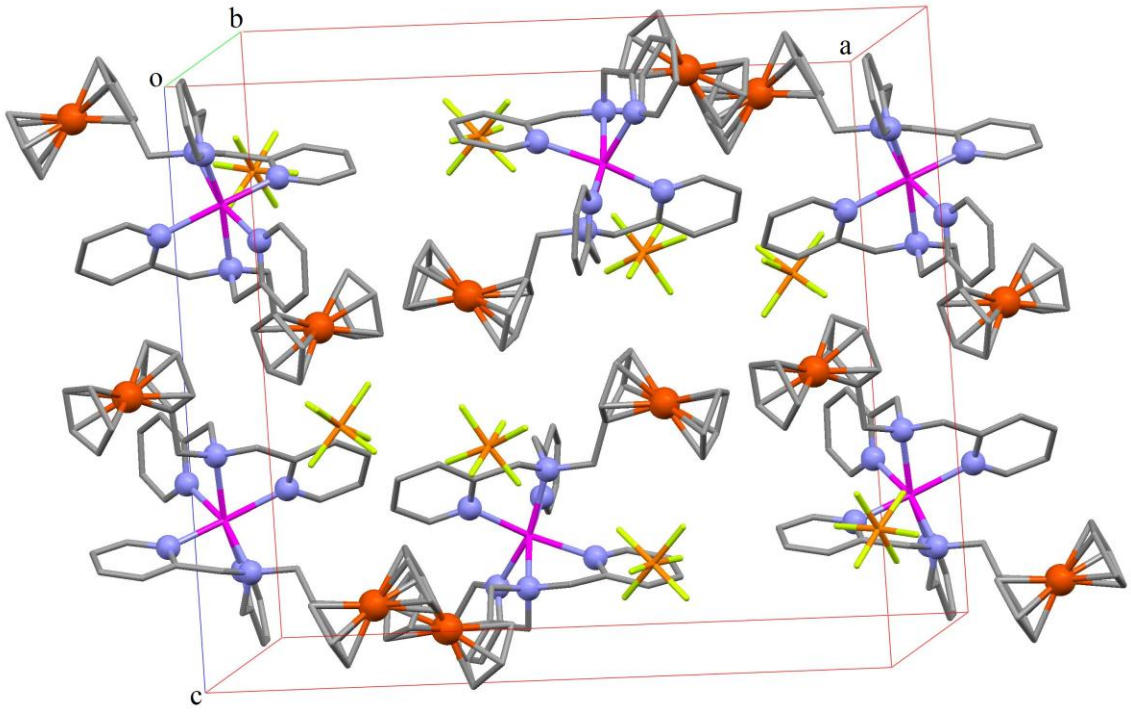

Figure S19: Unit cell packing diagram for the complex $[Zn(Fc\text{-}dpa)_2](PF_6)_2$. The complex crystallized in monoclinic *P*bcn space group with $Z = 4$. The hydrogen atoms are not shown for clarity.

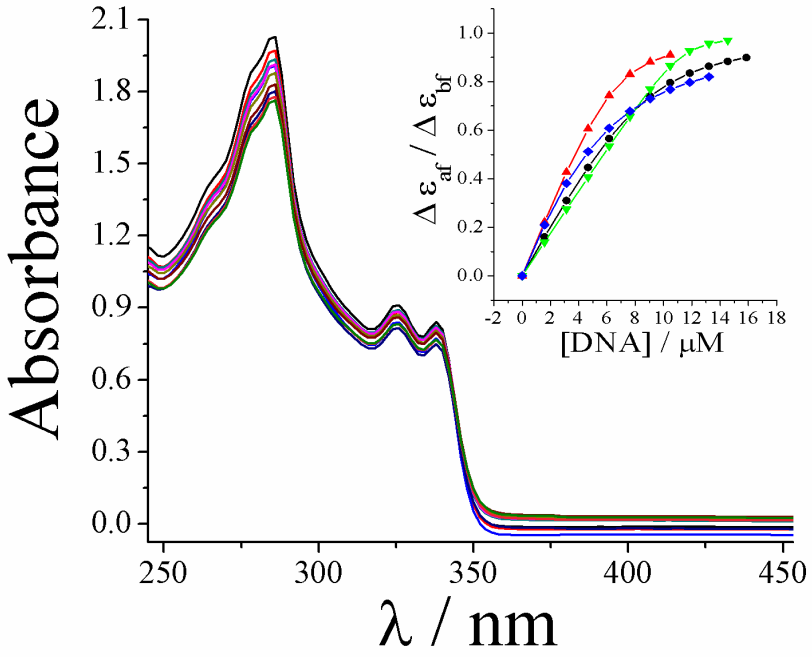

Figure S20. Spectral traces showing the effect of gradual addition of CT DNA (150 μM NP) to the 15-25 μM solution of the complexes in DMF-Tris-HCl buffer medium. The inset shows the best fit line plot of $\Delta\varepsilon_{af}/\Delta\varepsilon_{bf}$ vs. [DNA] for the complexes **1** (▲), **2** (♦), **3** (●) and **5**(▼).

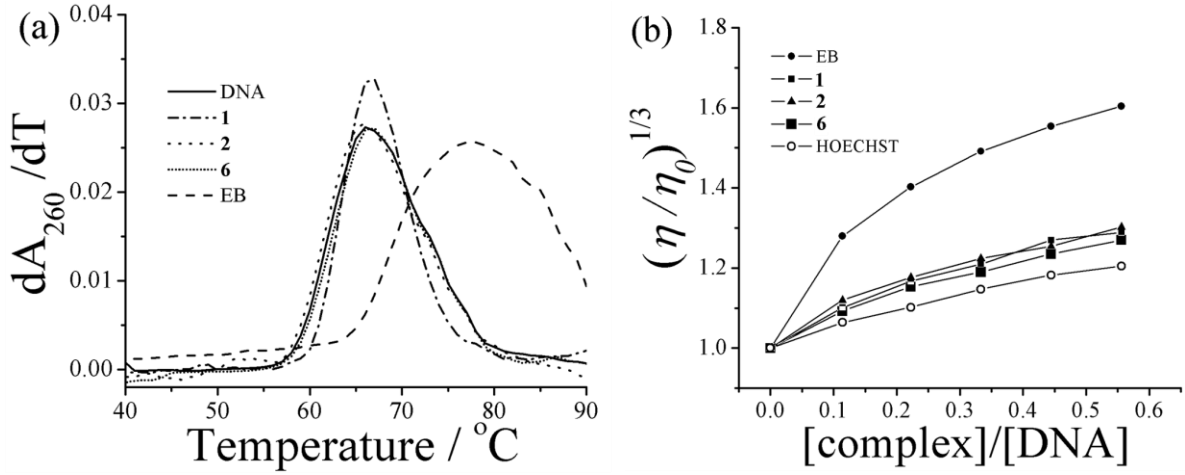

Figure S21. (a) DNA melting plots for the CT DNA (150 μM NP) alone and in the presence of the complexes **1**, **2** and **6** (15 μM) and ethidium bromide (EB, 15 μM) in 5 mM phosphate buffer (pH = 6.8). (b) The effect of addition of an increasing quantity of the complexes **1**, **2** and **6**, EB and Hoechst 33258 on the relative viscosity of CT DNA at 37.0 (±0.1) °C in 5 mM Tris-HCl buffer (pH = 7.2).

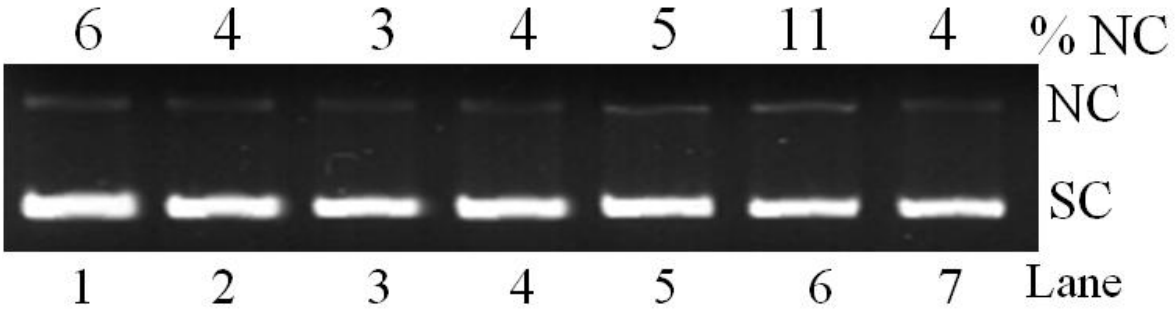

Figure S22. Gel electrophoresis diagram showing the DNA cleavage activity of **1** - **6** (20 μM) under dark condition using SC pUC19 DNA (0.2 μg, 30 μM b.p.) for an incubation time of 1 h: lane 1, DNA control; lanes 2-7, DNA + **1-6**, respectively**.**

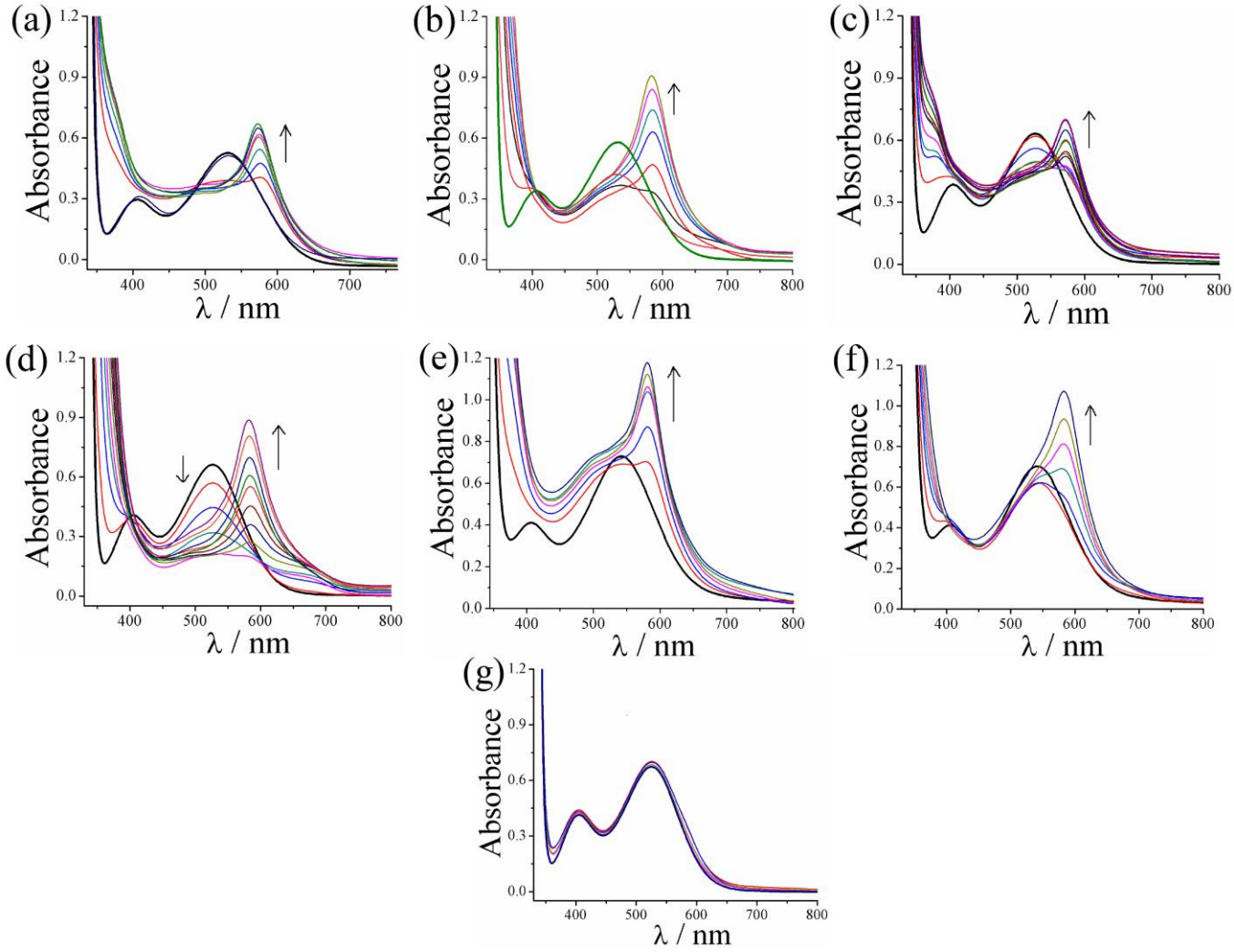

Figure S23. Absorption spectral changes of the complexes **3** and **4** under different experimental conditions: (a) photo-irradiation (3 min interval) of complex **4** in UV-A light of 365 nm in aqueous DMF, (b) complex **4** on treatment with ammonium ceric(IV) nitrate (30 mM stock solution in water) in aqueous DMF, (c) photo-irradiation (7 min interval) of complex **4** in UV-A light of 365 nm in aqueous acetonitrile, (d) complex **4** on treatment with ammonium ceric(IV) nitrate (30 mM stock solution in water) in aqueous MeCN, (e) photo-irradiation (3 min interval) of complex **3** in UV-A light of 365 nm in aqueous DMF, (f) complex **3** on treatment with ammonium ceric(IV) nitrate (30 mM stock solution in water) in aqueous DMF and (g) photo-irradiation (15 min interval) of complex **4** in UV light of 365 nm in pure acetonitrile. The thicker lines (black) indicate the spectra recorded at t = 0 min.

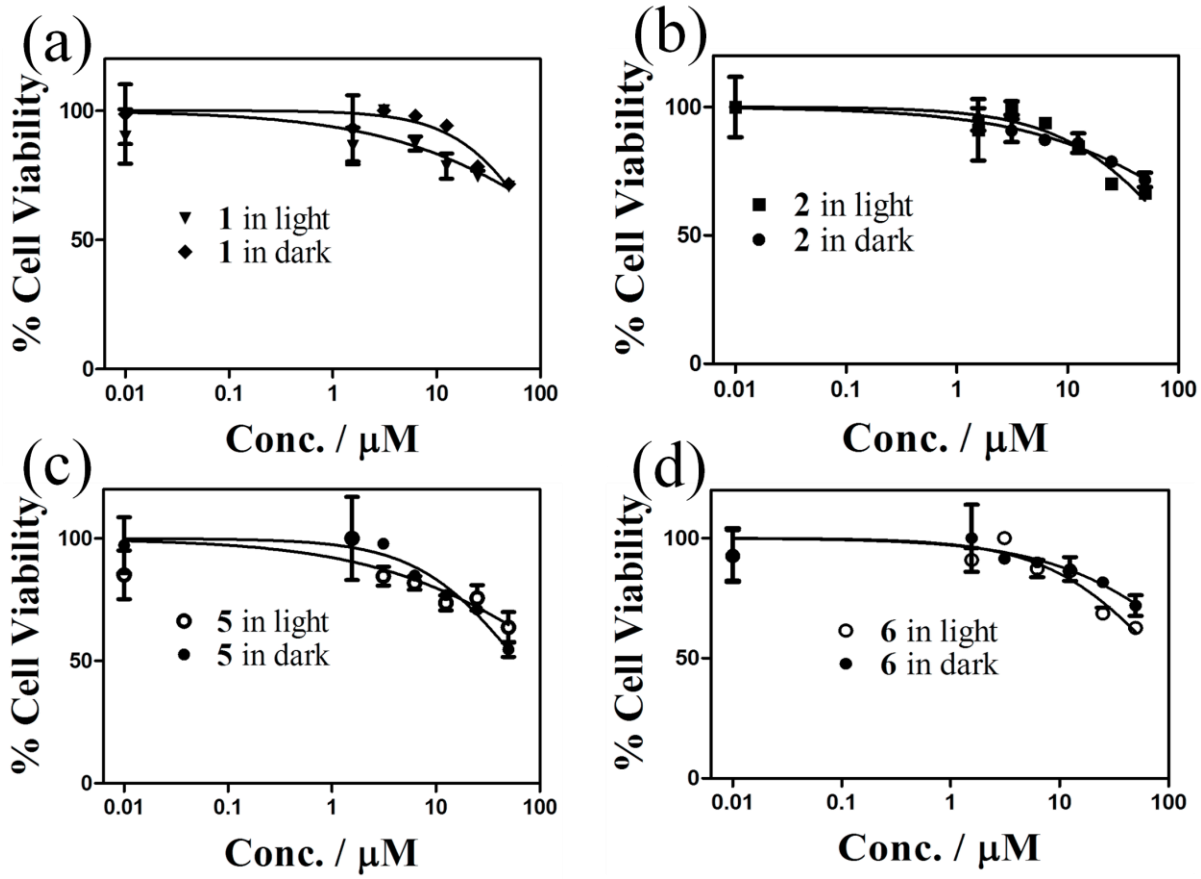

Figure S24. Photocytotoxicity of the complexes **1**, **2**, **5** and **6** in human cervical HeLa cancer cells on 4 h incubation in dark followed by photo-irradiation in visible light (400 to 700 nm) as determined by MTT assay.

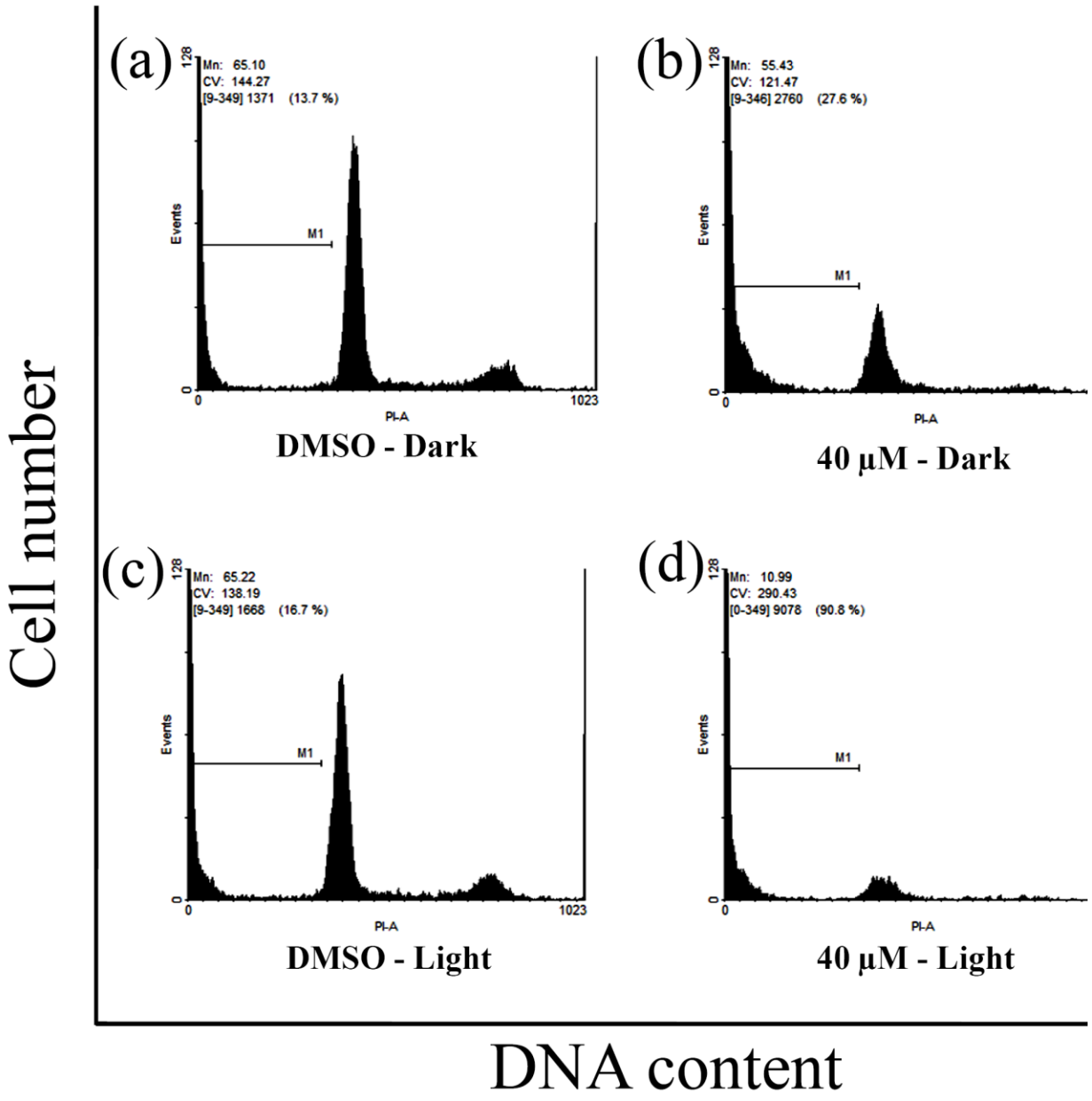

Figure S25. Complex **4** induced apoptotic cell death examined by flow cytometric analysis.